Identification of paleomagnetic remanence carriers in ca. 3.47 Ga dacite from the Duffer Formation, the Pilbara Craton

Identification of paleomagnetic remanence carriers in ca. 3.47 Ga dacite from the Duffer Formation, the Pilbara Craton

Yoichi Usui[a,*], Masafumi Saitoh[b], Kenichiro Tani[c], Manabu Nishizawa[d], Takazo Shibuya[d], Chie Kato[e], Tomoyo Okumura[f], Teruhiko Kashiwabara[g]

[a] *Volcanoes and Earth's Interior Research Center, Research Institute of Marine Geodynamics, Japan Agency for Marine-Earth Science and Technology (JAMSTEC), 2-15 Natushima-cho, Yokosuka, 237-0061, Japan*
[b] *Institut des Sciences de la Terre (ISTE), Faculté des géosciences et de l'environnement, Université de Lausanne (UNIL), Lausanne, Quartier Mouline, 1015 Lausanne, Switzerland*
[c] *Department of Geology and Paleontology, National Museum of Nature and Science, 4-1-1, Amakubo, Tsukuba-shi, Ibaraki 305-0005, Japan*
[d] *Institute for Extra-cutting-edge Science and Technology Avant-garde Research (X-star), Super-cutting-edge Grand and Advanced Research (SUGAR) Program, JAMSTEC, 2-15 Natushima-cho, Yokosuka, 237-0061, Japan*
[e] *Department of Environmental Changes, Faculty of Social and Cultural Studies, Kyushu University, 744 Motooka, Nishi-ku, Fukuoka 819-0395, Japan*
[f] *Center for Advanced Marine Core Research, Kochi University, Kochi 783-8502, Japan*
[g] *Submarine Resource Research Center, Research Institute for Marine Resources Utilization, JAMSTEC, 2-15 Natushima-cho, Yokosuka, 237-0061, Japan*

Abstract

The ca. 3.47 Ga Duffer Formation has been considered to carry one of the oldest paleomagnetic records. Yet, the lack of rock magnetic data limits the interpretation of the nature of the remanence. We conducted a rock magnetic and paleomagnetic investigation on columnar dacite of the Duffer Formation. The main magnetic minerals are phenocrysts of titanomagnetite and magnetite, and secondary hematite in groundmass. Detailed thermal

*Corresponding author
Email address: yoichi@jamstec.go.jp (Yoichi Usui)

demagnetization revealed more complex natural remanence than previously estimated, consisting of four components with typical unblocking temperature of $200-350$, $200-500$, 590, and 690 °C. Combined with alternating field demagnetization and rock magnetic data, they are attributed to titanomagnetite, coarse-grained magnetite, fine-grained magnetite, and hematite, respectively. The comparison of unblocking temperature and coercivity suggest that the previously proposed secondary component is carried by fine-grained magnetite as well as hematite, while the putative primary component is carried by coarse-grained magnetite and titanomagnetite. Microscopic observations showed that coarse-grained magnetite and titanomagnetite are primary crystals, although this does not necessarily indicate they preserve primary remanence. The remanence directions of all components revealed higher scatter than the previous studies, suggesting the need for caution in interpretation. The low unblocking temperature of tittanomagnetite suggests that if their remanence is truly primary, the rocks must have kept below $\sim$250 °C for $\sim$3.47 billion years.

Keywords: the oldest remanence; magnetic minerals; titanomagnetite

1. Introduction

The existence of the geomagnetic field in the early history of the Earth places important constraints on its thermal evolution (e.g. Davies et al., 2015). Nonetheless, the persistence of the geomagnetic field for more than 3 billion years has been deduced only from a few paleomagnetic studies. Paleomagnetic data for rocks older than 3.2 Ga comes mostly from the Pilbara craton in Western Australia (McElhinny & Senanayake, 1980; Suganuma et al.,

2006; Bradley et al., 2015; Herrero-Bervera et al., 2016) and the Kaapvaal craton of South Africa (Hale & Dunlop, 1984; Layer et al., 1996; Yoshihara & Hamano, 2004; Tarduno et al., 2007; Usui et al., 2009; Biggin et al., 2011). Of these, even smaller number of studies constrain the age of the magnetic remanence using paleomagnetic field test (McElhinny & Senanayake, 1980; Usui et al., 2009; Biggin et al., 2011).

McElhinny & Senanayake (1980) claimed a positive fold test using columnar dacite and pillow basalt of the Duffer Formation of the Pilbara Craton. The columnar dacite was dated as 3.467 ± 0.005 Ga (Nelson, 2001), and the paleomagnetic result has been taken as evidence for the existence of the geomagnetic field at $\sim$3.5 Ga. However, there is a debate about this interpretation (Tarduno et al., 2007; Usui et al., 2009; Schmidt, 2014). Particularly, rock magnetic data were very limited, preventing the discussion about remanence acquisition mechanisms. McElhinny & Senanayake (1980) identified two remanence components and one transient component in both alternating field (AF) and thermal demagnetization of the columnar dacite. The putative primary component, labelled here as DFM, was observed at intermediate temperature ($\sim$250$-$500 °C) and coercivity ($\sim$10$-$40 mT). At higher temperature and coercivity, they identified another component that failed the fold test (labelled as DFH). In thermal demagnetization, DFH extended above 640 °C, suggesting hematite as a carrier. However, in AF demagnetization, DFH was fitted from $\sim$40 mT. This is rather low coercivity for hematite, leaving a question about the carrier. Recently, Herrero-Bervera et al. (2016) conducted a rock magnetic and paleointensity study using similar dacitic rocks of the Duffer Formation. Their sampling locality does not show colum-

nar joints (their figure 2), so it is probably not the same site with McElhinny & Senanayake (1980) although it is close (Herrero-Bervera, personal communication). Nonetheless, Herrero-Bervera et al. (2016) showed that the dacite exhibits three Curie temperatures of ∼150, 450, and 580 °C. These temperatures also mark directional changeover points of natural remanence upon progressive thermal demagnetization, and the highest blocking temperature component (450 − 580 °C), which was not identified by McElhinny & Senanayake (1980), was interpreted as a candidate for primary remanence. A similar direction was isolated in AF demagnetization at above 30 mT. This is also higher than the coercivity range of the DFM, but rather similar to the coercivity of DFH. Notably, Herrero-Bervera et al. (2016) did not observe hematite contribution in their samples. This suggests a possibility that DFH may be partly carried by magnetite, and that DFM may be contaminated by, or even an artifact of, overlapping magnetization of DFH and a transient component (Tarduno et al., 2007). However, in the absence of detailed rock magnetic data, it is not clear if the columnar dacite of the Duffer Formation also contains a distinct component unblocks between ∼450 − 580 °C.

The paleomagnetic data of the Duffer Formation (McElhinny & Senanayake, 1980) are also pivotal to other studies of rocks from the Pilbara Craton. Rapid Archean plate motion of the Pilbara craton was proposed on the basis of the comparison among the Duffer Formation data and the data from the slightly younger Marble Bar Chert Member (Suganuma et al., 2006). Bradley et al. (2015) compared the paleomagnetic directions obtained from basalt of the Coucal Formation (∼3.51 Ga) and the Euro Basalt (∼3.34 Ga) with the Duffer Formation data to propose that the Coucal Formation remanence pre-

date ∼3.34 Ga. These studies rely on the interpretation that the remanence of the Duffer Formation dacite is almost the same age with the rock itself. Because of its importance in understanding the early history of the geomagnetic field and tectonics, we revisit the Duffer Formation columnar dacite for an additional rock magnetic and paleomagnetic investigation.

2. Geology

The study area locates southwest of a town Marble Bar and near the Glen Herring Gorge, surrounded by granitic complexes (the Mount Edgar Complex, the Shaw Complex, and the Corunna Downs Complex) (Figure 1). Dacite with columnar joints is cropping out on the northern end of the Archean succession, along small creek over an area of approximately 500 m × 500 m (Figure 2). Dacitic volcanic breccia is in the southwest of the area, which is interpreted to be stratigraphically above the columnar dacite (Hickman & Van Kranendonk, 2008). The boundary between the columnar dacite and the volanic breccia was not well exposed, but transition was clear without any interbedding. The strike of the lithologic transition was approximately 315°, which agrees with the bedding strike estimated from the local columnar joint (∼310°) and regional strike of the Duffer Formation (∼300°) (McElhinny & Senanayake, 1980; Hickman & Van Kranendonk, 2008). To the north, the columnar dacite is unconformably overlaid by basalt of the Fortescue Group (∼2.72 − 2.78 Ga) (Arndt et al., 1991). A few basaltic dykes intrude the columnar dacite near the boundary with the Fortescue basalt. Our sampling sites are adjacent to the locality of Nelson (2001). We note that the sampling locality of McElhinny & Senanayake (1980), which

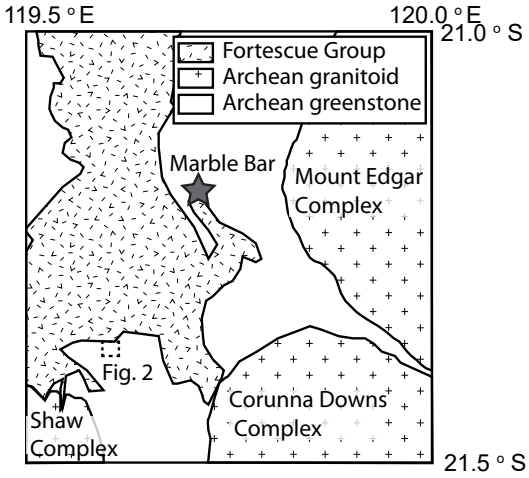

Figure 1: Simplified geological map showing sampling area.

was originally presented in Pidgeon (1978) as (21°21′25″ S, 119°36′11″E), would be ∼800 m to the north from our sampling sites, and it falls within the Fortescue Group. This is probably an inevitable error before the GPS era.

3. Methods

3.1. Sampling and magnetic susceptibility mapping

Samples of the columnar dacite were collected either by hand or using engine drills (Figure 2, Table 1). Sample orientations were determined using magnetic compass, which was checked against sun compass when possible. Magnetic susceptibility was mapped in the field using SM30 (ZH instruments).

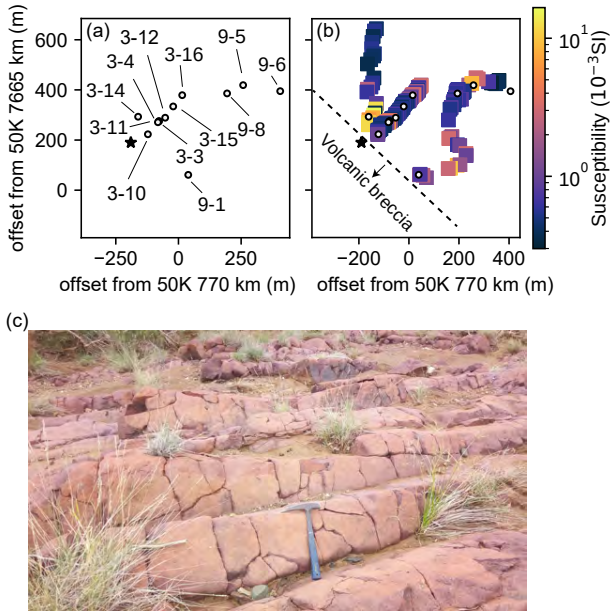

Figure 2: Sampling locations (a) and magnetic susceptibility distributions (c). X and Y coordinates shows distance in m from a reference point 50 K 770000 m E, 7665000 m S in UTM coordinate. Black star shows the sampling locality for the geochronological study of Nelson (2001). (c) Typical outcrop of the columnar dacite.

Table 1: List and magnetic magnetic characteristics of sites analyzed in this study.

Site	latitude (°)	longitude (°)	specimen N	MS (m S.I.)	IRM (A/m)			NRM components	comment
					0 - 0.12 T	0.12 - 0.4 T	0.4 - 2.7 T		
GL9-5	-21.36317	119.60611	3	0.637	0.42	3.98	5.23	LC, MC, HMC, HC	1 core
GL3-12	-21.36439	119.60313	5	0.661	1.21	4.28	5.88	LC, MC, HC	2 cores and 1 hand sample
GL3-15	-21.36425	119.60344	12	0.747	0.77	2.38	3.17	LC, MC, HC	1 hand sample
GL3-3	-21.36452	119.60289	10	1.06	1.58	1.55	2.02	univectorial	1 hand sample
GL9-8	-21.36347	119.60550	10	1.14	6.69	3.57	3.47	LC, MC, HMC	1 hand sample
GL9-1	-21.36643	119.60405	8	1.26	5.07	3.37	5.96	HC	1 hand sample
GL3-10	-21.36500	119.60248	3	1.38	21.98	8.26	8.32	HC	1 core
GL3-16	-21.36356	119.60377	6	4.29	17.56	5.57	3.38	LC, LMC, HMC	2 cores and 1 hand sample
GL9-6	-21.36336	119.60754	8	6.19	47.03	2.05	0.82	univectorial	1 hand sample
GL3-11	-21.36455	119.60286	5	6.56	40.62	9.45	5.57	LC, LMC, HMC	3 cores
GL3-4	-21.36452	119.60289	13	14.7	16.65	1.35	2.27	univectorial	1 hand sample
GL3-14	-21.36427	119.60216	10	24.4	75.75	6.09	7.59	univectorial	2 cores

specimen N: number of specimen; MS: bulk magnetic susceptibility

3.2. Rock magnetism and microscopy

We measured volume specific bulk magnetic susceptibility, temperature dependence of susceptibility $\kappa(T)$, demagnetization of triaxial isothermal remanence (IRM) (Lowrie, 1990), and coercivity distribution. Bulk susceptibility was measured by a Kappa Bridge KLY-4 (AGICO) for standard 10.5 cc cylindrical specimens. $\kappa(T)$ was measured by the KLY-4 with a furnace CS-3. Powdered samples were heated in flowing Ar up to 700 °C and subsequently cooled to 50 °C. Orthogonal IRM was imparted by fields of 2.7, 0.4, and 0.12 T using a pulse magnetizer Model 660 (2G Enterprises). Then the triaxial IRMs were subjected to progressive thermal demagnetization with a thermal demagnetizer TDS-1 (Natsuhara Giken). Remanence was measured with a spinner magnetometer ASPIN (Natsuhara Giken). Coercivity distribution was estimated using backfield demagnetization of IRM and first-order reversal curves (FORCs) measured by a vibrating sample magnetometer (VSM) Model 29/3902 (Princeton measurements). IRM was imparted at 1 T, and progressively demagnetized by backfields from -0.5 mT to -1 T in non-linear field steps. FORCs were also analyzed to estimate the backfield coercivity distributions. Measurements were performed with saturation field of 0.5 T and field increments of 2 or 3 mT. FORC diagrams and backfield demagnetization were calculated using software VARIFORC ver. 4.01(Egli, 2013). The backfield analysis from FORCs uses more measurement points than the traditional method (Egli et al., 2010), and give better resolution of coercivity distribution below 0.1 T for the samples dominated by high coercivity minerals (see results).

Polished thin sections were prepared from selected samples and examined

with scanning electron microscope (SEM) Quanta 450 FG (FEI) equipped with an energy-dispersive X-ray spectroscopy (EDS) system Elite Plus (Ametek).

3.3. Paleomagnetism

When available, two pilot specimens were subjected to detailed AF and thermal demagnetization from each site. AF demagnetization was conducted using a demagnetizer DEM95 with two axes tumbling, and thermal demagnetization was conducted using the TDS-1. Remanence was measured using the spinner magnetometer ASPIN. Based on the pilot results, the remaining specimens were treated in thermal demagnetization, or thermal demagnetization preceded by AF demagnetization at low fields. Demagnetization results were examined using principal component analysis (Kirschvink, 1980) using software PuffinPlot (Lurcock & Wilson, 2012).

4. Results

4.1. Magnetic susceptibility mapping

Magnetic susceptibility showed significant spatial variation by a factor of ∼50 even within apparently massive columnar dacite (Figure 2). The variation did not extend laterally along the bedding. Our samples cover most of the susceptibility variation. Susceptibility measured at field was generally consistent with the bulk susceptibility measured on specimens (Table 1).

4.2. Rock magnetism and microscopy

$\kappa(T)$ showed variety of patterns (Figure 3). Overall, sharp decrease upon heating was observed at ∼150, 380, 590, and 690 °C with variable magni-

tudes. The variation correlates partly with bulk susceptibility such that samples with high bulk susceptibility showed dominant change at ∼590 °C. The cooling curves were generally above the heating curve. Samples with high bulk susceptibility showed relatively small alteration due to the heating. The change at∼150 °C disappeared upon heating, the change at ∼590 °C generally increased, and the heating and cooling curves above ∼600 °C were nearly identical.

Thermal demagnetization of triaxial IRM indicated the presence of three unblocking temperatures at ∼350, 590, and 690 °C (Figure 4). The high coercivity (0.4 - 2.7 T) and middle coercivity (0.12 - 0.4 T) IRM mainly unblocked at ∼690 °C, with smaller change at ∼300 - 400 °C. The low coercivity IRM (< 0.12 T) decayed rapidly to ∼350 °C, and then unblocked almost completely at ∼580 °C. Among sites, the magnitude of the low coercivity IRM varied from 0.425 A/m (GL9-5) to 75.7 A/m (GL3-14), and it correlates well with bulk magnetic susceptibility (Table 1). The magnitude of high coercivity IRM showed smaller variation from 0.82 A/m (GL9-6) to 8.32 A/m (GL3-10). The magnitude of high and low coercivity IRMs were not correlated.

Backfield coercivity distributions also correlated with magnetic susceptibility. There were high coercivity phases that did not saturate at 1 T, together with phases with peak coercivities less than 100 mT (Figure 5). The high coercivity phases were dominant in low susceptibility samples. Below 100 mT, the coercivity distributions of GL3-4 and GL9-6 exhibited maxima at lower field (10 - 15 mT) than the other samples (50 - 60 mT). In addition, the IRM gradients of GL3-11 and GL9-8 showed a bump at ∼10 mT, indi-

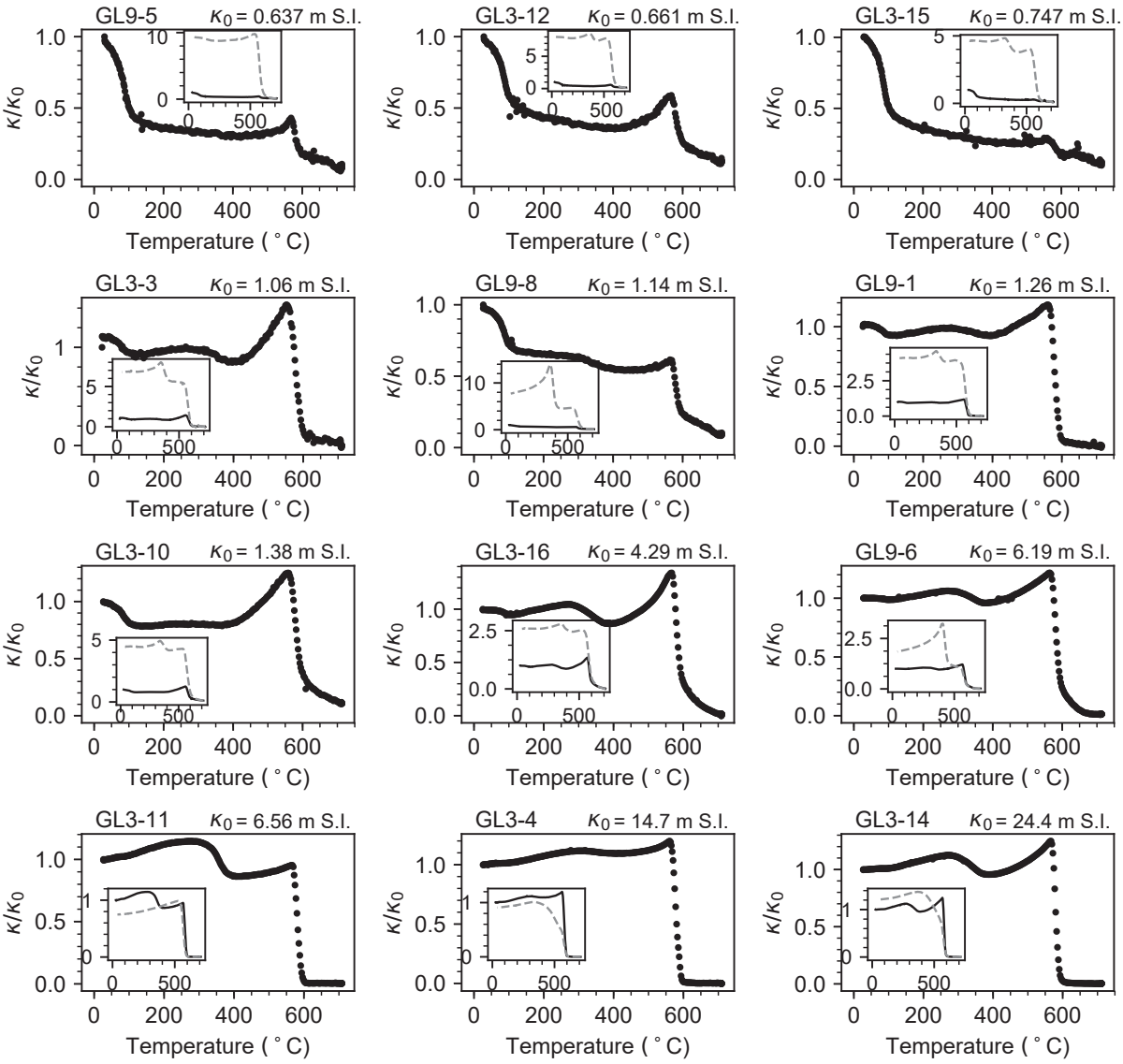

Figure 3: Temperature dependence of magnetic susceptibility. Data are normalized by room temperature susceptibility κ_0. Results are ordered in ascending bulk susceptibility of the sites, which is indicated on the upper right of each plot. Insets show heating and cooling curves in black and gray, respectively.

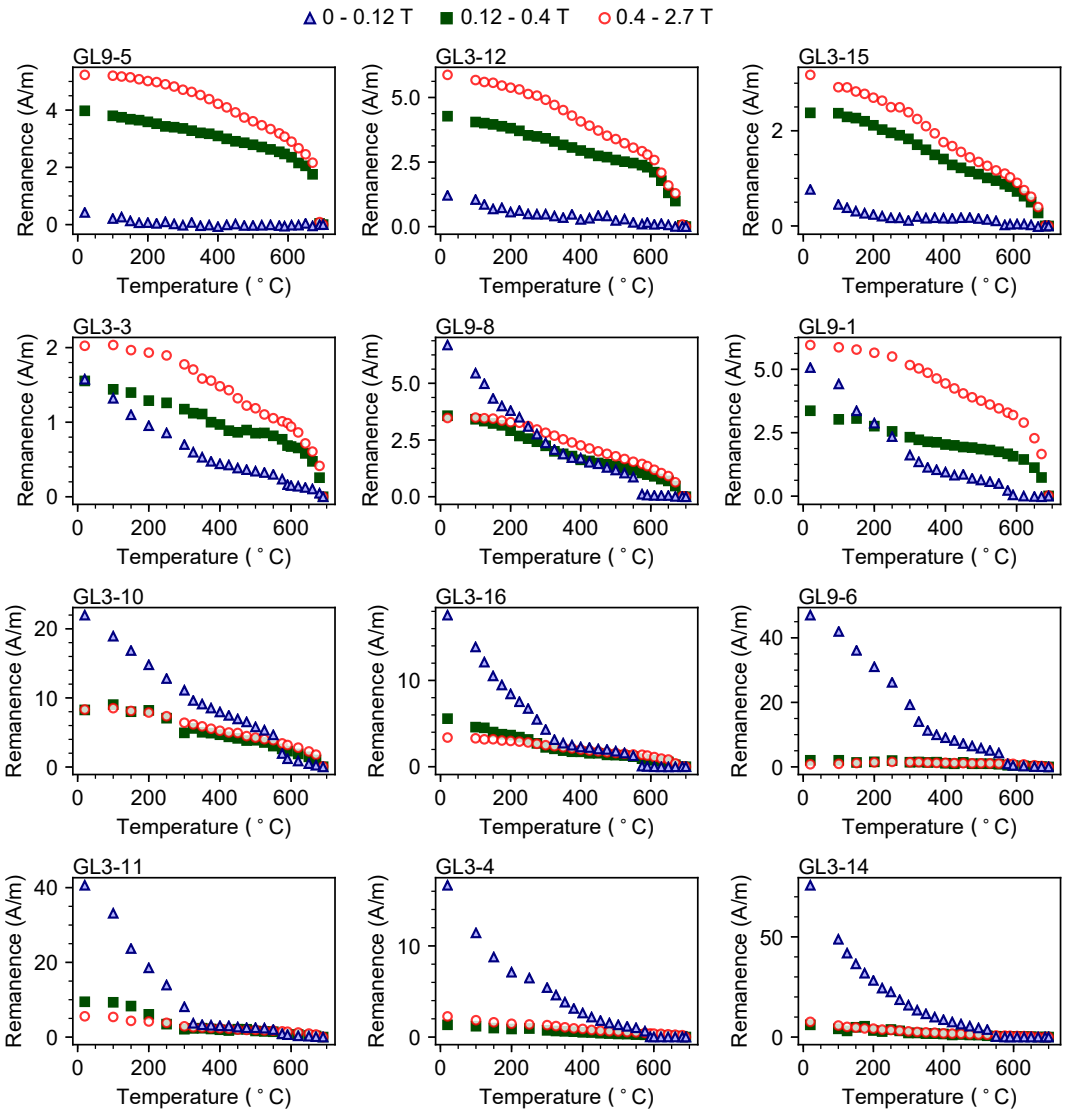

Figure 4: Progressive thermal demagnetization of triaxial IRM. Red circles represent high coercivity IRM (0.4 - 2.7 T), green squares middle coercivity (0.12 - 0.4 T), and blue triangles low coercivity (0 - 0.12 T). Results are ordered ascending bulk susceptibility of the sites as in figure 3.

cating the mixing of coercivity distributions with peaks at ∼10 mT and ∼60 mT. The samples with large contributions of the high coercivity phases were further examined through FORC diagrams and backfield coercivity distribution based on FORC measurements (Figure 6 and 7). The FORC diagrams below 0.2 T are similar regardless of the bulk susceptibility, and coercivity distribution indicate a peak at around 30-50 mT. These results showed that samples dominated by high coercivity phases also contain phases with peak coercivity < 100 mT.

SEM observations were conducted on samples with contrasting rock magnetic characteristics (GL3-4, 3-10, 3-12, 3-14, 3-16, 9-5, and 9-8). Two major modes of occurrence of iron oxides were observed: homogeneous but fragmented large grains and irregular intergrowth with Ti oxide (Figure 8a). These occurrences were common among the examined samples. Occasionally grains contain texture similar to the trellis-type lamellae of high temperature oxidation was observed (Figure 8b). Such grains are generally highly degraded. Iron oxides were often rimed by secondary mafic minerals, which in turn rimed by iron oxides (Figure 8b). It is unclear if those surrounding oxides are relict of the primary minerals, or secondary overgrowth. EDS analyses showed that homogeneous grains and grains with trellis-type lamellae contain only small amount of Ti, while iron oxide showing irregular intergrowth with Ti-oxide revealed elevated Ti/Fe of ∼0.14 (average of 21 spots in 8 grains; standard deviation is 0.1).

4.3. Paleomagnetism

As expected from rock magnetic results, paleomagnetic characteristics were also variable. The sites GL3-3, 3-4, 3-14, and 9-6 revealed nearly uni-

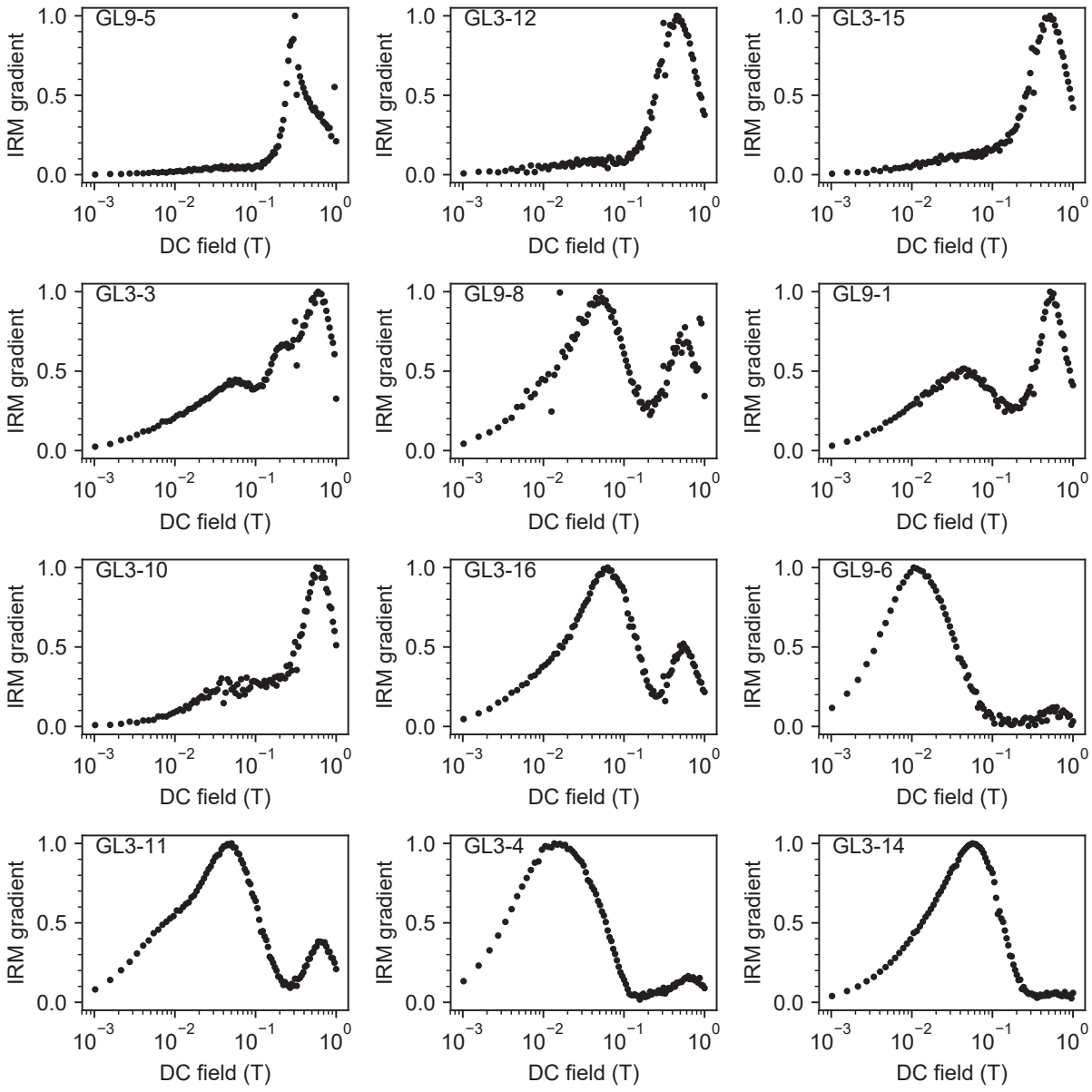

Figure 5: Coercivity distribution estimated by backfield demagnetization of IRM. Data are normalized by the maximum IRM gradient. Results are ordered ascending bulk susceptibility of the sites as in figure 3.

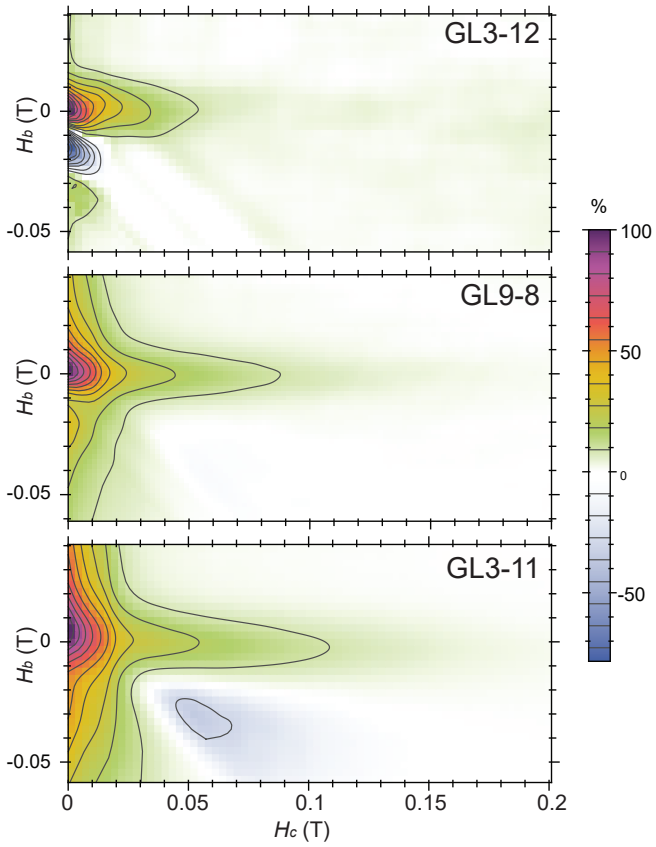

Figure 6: Representative FORC diagrams for samples with contrasting bulk susceptibility.

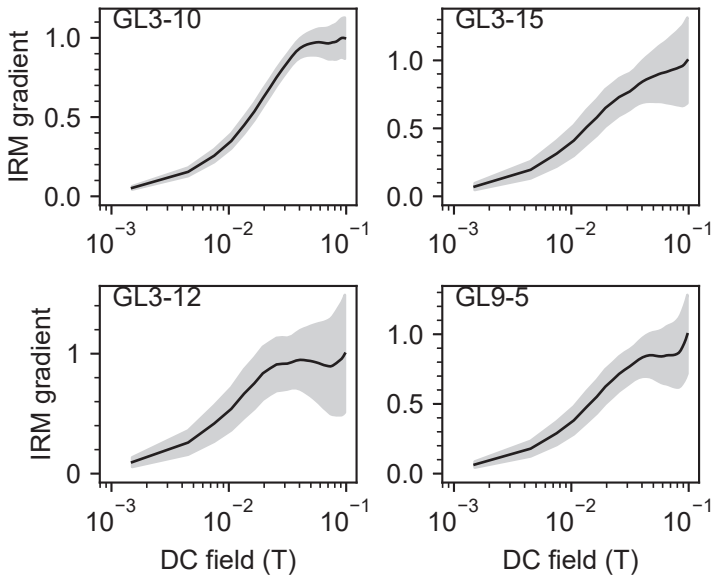

Figure 7: Coercivity distribution estimated by FORC measurements (Egli et al., 2010) for high coercivity samples. Data are normalized by the maximum IRM gradient below 100 mT. Gray shaded area represent standard error multiplied by 2.

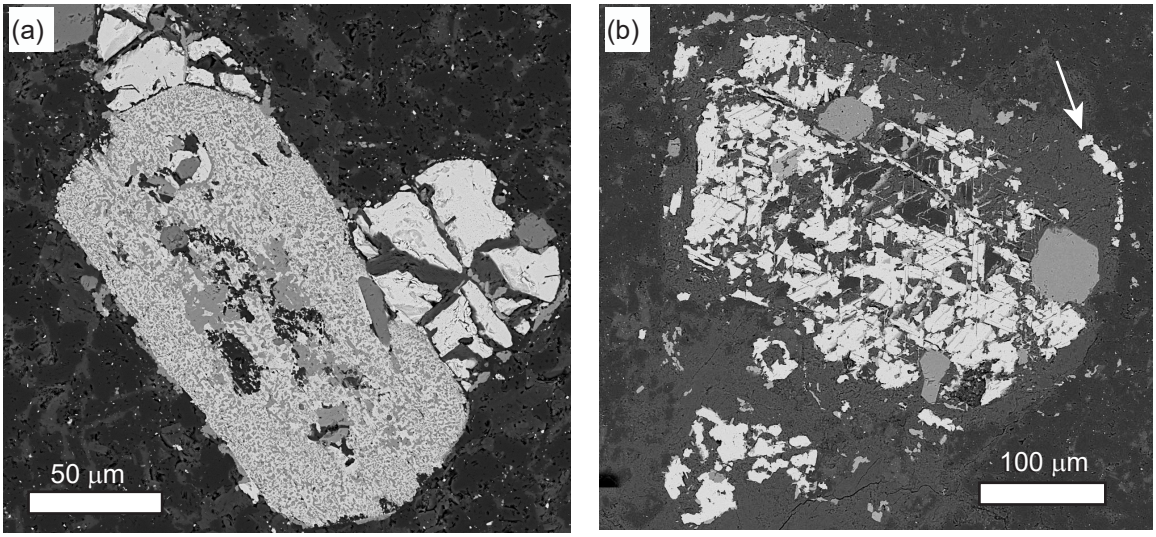

Figure 8: Representative back scattered electron images. (a) Image of homogeneous grains and a grain with irregular internal structure. EDS analyses shows the homogeneous grains are Fe oxide, while the irregular grain is intergrowth of Ti oxide and Fe-Ti oxide. (b) Grain with trellis-type lamellae. Arrow indicates the iron oxide on surrounding mafic mineral.

vectorial remanence in both AF and thermal demagnetization (Figure 9). We consider that these sites were completely remagnetized, most probably by recent lightning strikes. GL3-10 and GL9-1 revealed only two components separated at 590 °C. We interpret that these sites were also remagnetized, with a high coercivity component carried by hematite barely survived the remagnetization. The other sites revealed more than one component below 590 °C, and their behavior roughly correlated with rock magnetic properties. One site (GL3-12) with low bulk susceptibility revealed behavior similar to the thermal demagnetization result presented by McElhinny & Senanayake (1980); a low temperature component unblocked by ∼200 °C, an intermediate temperature component between ∼300 - 500 °C, and a high temperature component above ∼600 °C (Figure 9). We will call these three components as LC, MC, and HC, respectively. AF demagnetization of the sample GL3-12 failed to separate LC and MC, with remanence approached non-zero end-point by ∼30 mT, indicating that MC was carried by relatively low coercivity phases (Figure 9). In contrast, two samples (GL3-11, and 3-16) with high bulk susceptibility revealed three components below 600 °C, and unblocked almost completely by 600 °C (Figure 9). This behavior is similar to the results of Herrero-Bervera et al. (2016). The first component unblocked by ∼200 °C, and we will also call this component as LC. The remaining two components unblocked at ∼250 - 350 °C and ∼500 - 590 °C, respectively. We will call these two components as LMC and HMC, respectively. AF demagnetization of GL3-16 revealed directions similar to LC, LMC, and HMC at 0 - 5, 5 - 60, and 60 - 150 mT, respectively (Figure 9). Interestingly, this behavior is similar to the AF demagnetization result of McElhinny & Senanayake (1980).

They classified a component demagnetized in 5 - 40 mT as DFM, and 40 - 200 mT as DFH. Because they only presented single demagnetization plot, it is not clear whether that was a typical behavior, or whether these components were also recovered in thermal demagnetization. Here, we distinguish LMC and HMC from MC or HC because their unblocking temperatures are clearly different. Note that LMC and MC did not coexist in a single sample. Typical characteristics of the components are summarized in Table 2.

Table 2: Summary of NRM components.

Component	T_B	H_C	Potential carrier	comment
LC	$< 200\,^{\circ}\mathrm{C}$	< 5 mT	(titano)magnetite?	H_C overlaps with MC
MC	$300 - 500\,^{\circ}\mathrm{C}$	< 30 mT	(titano)magnetite	H_C overlaps with LC
HC	$600 - 690\,^{\circ}\mathrm{C}$	> 150 mT	hematite	
LMC	$250 - 350\,^{\circ}\mathrm{C}$	$5 - 60$ mT	titanomagnetite	
HMC	$500 - 590\,^{\circ}\mathrm{C}$	$60 - 150$ mT	magnetite	

T_B: Blocking temperature; H_C: coercivity

The other samples can be described by the combination of LC, MC, HMC, and HC. Site GL9-5 showed LC, MC, HMC, and HC and GL9-8 showed LC, MC, and HMC. HMC and MC of these sites overlapped significantly, and AF demagnetization cannot discriminate MC and HMC (Figure 9). The site GL3-15 was complicated. It exhibited three components LC, MC, and HC similarly to GL3-12, but some specimens from GL3-15 revealed HC directions nearly antipodal to those from the other specimens from the same site, even though we only measured single hand sample of ∼20 cm size from GL3-15 (Figure 9).

We filtered specimen data for maximum angular dispersion (MAD) smaller than 15° or 20° to calculate site mean directions (Figure 10; Table 3). While within-site dispersion was reasonable, the inter-site dispersion is was very large, preventing the calculation of study mean directions for any components.

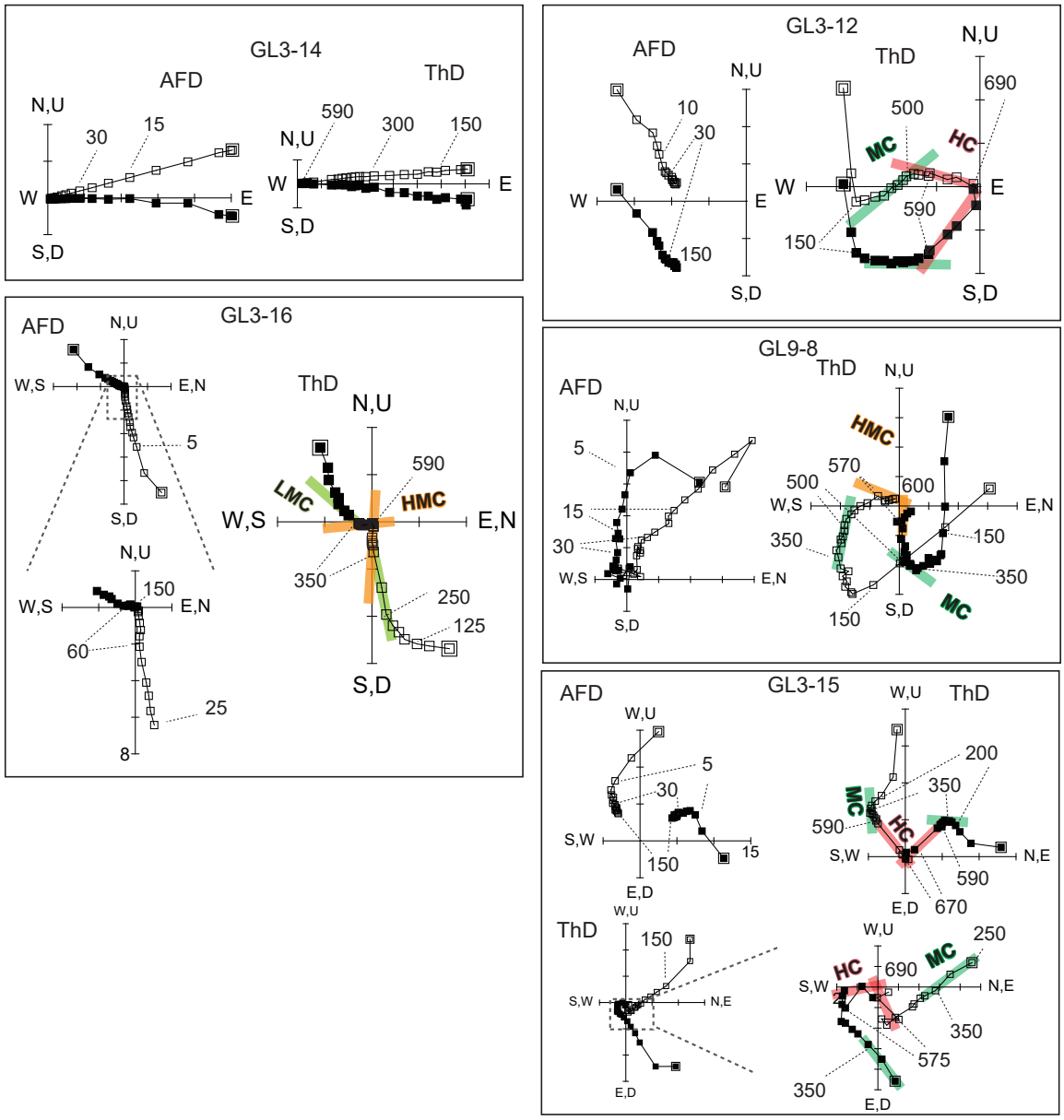

Figure 9: Representative orthogonal vector plots. Filled symbols represent horizontal projection, and open symbols represent vertical projection. Numbers indicate the demagnetization steps in mT for AF demagnetization (AFD), or in °C for thermal demagnetization (ThD).

Table 3: Site mean directions

Site	Declination	Inclination	n	k	α_{95}	comment
			MC			
GL3-12	-77.7	30.89	5	73.94	8.96	
GL3-15	-0.52	-26.78	6	7.23	26.74	
GL3-15*	-20.15	-27.02	4	24.75	18.84	without two possible outlier
GL9-5	-24.26	-52.21	1	NA	NA	
GL9-5*	-168.24	-50.67	2	10.53	NA	MAD $< 20°$
GL9-8	148.77	8.68	4	41.44	12.62	
GL9-8*	148.07	15.93	6	11.79	20.35	MAD $< 20°$
			HC			
GL9-1	-111.28	-28.04	4	207.53	6.39	
GL9-5	158.81	-16.66	2	31.24	NA	
GL3-15	-38.96	-40.16	7	61.44	7.76	antipodal directions were inverted
GL3-12	-137.96	-10.21	6	234.38	4.39	
GL3-12*	-141.33	-10.9	8	53.62	7.63	MAD $< 20°$
GL3-10	81.88	-21.17	2	385.93	NA	
			LMC			
GL3-11	-131.53	-0.58	3	3.36	82.46	
GL3-11*	-142.81	18.85	2	377.63	NA	without one possible outlier
GL3-16	-51.74	69.72	5	221.8	5.15	
			HMC			
GL3-11	-128.87	-17.25	3	13.85	34.46	
GL3-16	-94.87	60.32	5	55.97	10.32	
GL9-8	176.79	-18.03	3	21.33	27.38	

n: Number of specimen used for calculation; k: Fisherian concentration parameter; α_{95}: 95% Fisherian confidence limit.

5. Discussion

5.1. Magnetic Mineralogy

Rock magnetic data showed that the columnar dacite exhibits a gradation of behavior between two end-members: (1) higher susceptibility and lower coercivity samples with dominant blocking temperatures at ∼350 and ∼590 °C, and (2) lower susceptibility and higher coercivity samples with a dominant blocking temperature at ∼690 °C (Figures 3-7). The high coercivity and high blocking temperature phase is interpreted as hematite, and the blocking temperature at ∼590 °C as magnetite. Titanomagnetite and magnetite were observed under SEM. Titanomagnetite shows an average Ti/Fe ratio of ∼0.14. Assuming titanomagnetite without maghemitization, this average Ti content corresponds to a Curie temperature of 360 °C (Bleil & Petersen, 1982). So, we interpret that the unblocking temperature of ∼350 °C reflects the Curie temperature of titanomagnetite.

Microscopic observations indicate that the majority of (titano)magnetite were originally crystallized from magma as phenocrysts (Figure 8). The magnitude of low coercivity (< 0.12 T) IRM varies much more compared to high coercivity (> 0.4 T) IRM. Such behavior is simply explained by the abundance variation of the (titano)magnetite phenocrysts against relatively uniform hematite background. This interpretation is consistent with the petrologic observation that hematite is dispersed within groundmass (Nelson, 2001). The presence of (titano)magnetite phenocrysts is indicative of secondary origin of hematite, yet the exact formation process is not clear. Considering the good correlation among IRM intensity, unblocking temperature, and coercivity (3-7; Table 1), the abundance variation of (titano)magnetite

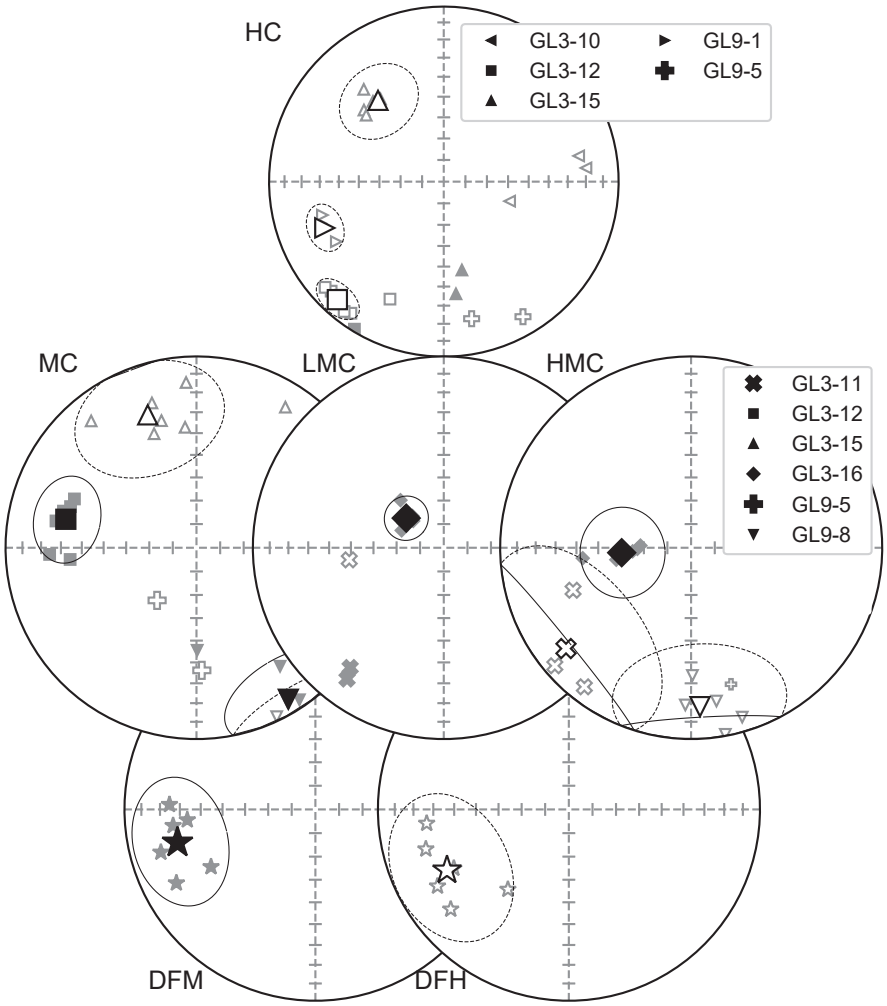

Figure 10: Equal area projection of PCA directions. Small gray symbols in HC, MC, LMC, and HMC represent specimen data. Site mean directions are shown in large symbols for sites with sample number larger than 2, together with 95% Fisherian confidence limit shown as dashed cones. Filled symbols represent lower hemisphere projection, and open symbols represent upper hemisphere projection. Also shown are the mean direction of DFM and DFH of (McElhinny & Senanayake, 1980), together with 95% Fisherian confidence limit shown as dashed cones. Small gray symbols represent site mean directions.

phenocrysts is the main mechanism to cause the rock magnetic variations within the columnar dacite.

SEM observations and triaxial IRM analyses showed that titanomagnetite and magnetite co-occur regardless of the total abundance of (titano)magnetite phenocrysts (Figures 4 and 8). The relative abundance between titanomagnetite and magnetite may be qualitatively estimated from $\kappa(T)$ curves by comparing the decrease at ∼350 °C and ∼590 °C. (Figure 3). When compared with coercivity distributions (Figure 5), there is a tendency that samples with higher contribution of magnetite exhibit lower coercivity (i.e., GL3-4 and GL9-6), indicating that magnetite has lower coercivity than titanomagnetite on average. This is supported by SEM observations showing titanomagnetite as fine intergrowth with Ti oxide, while most magnetite as large, discrete grains. The $\kappa(T)$ curves for the samples with low magnetic susceptibility show clear decrease at ∼590 °C and ∼700 °C but not at ∼350 °C, suggesting that these samples contain small amount of titanomagnetite relative to magnetite.

5.2. Paleomagnetism

Rock magnetic data corroborated with microscopic observations show that the columnar dacite in the Duffer Formation generally contains three magnetic minerals of titanomagnetite, magnetite, and hematite. Their responses to progressive demagnetizations should be different. Specifically, thermal demagnetization by 400 °C should eliminate the contribution from titanomagnetite, and above 600 °C the only hematite contribution would be isolated. AF demagnetization would preferentially diminish the contribution from large magnetite. We combine this information with paleomagnetic

results to infer the paleomagnetic remanence carriers.

5.2.1. Hematite component (HC)

HC unblocks above 600 °C, and is hardly demagnetized up to 150 mT (Figure 9; Table 2), indicating that this component is carried by hematite. McElhinny & Senanayake (1980) interpreted that their DFH component is carried by hematite, so one would expect the HC direction to be close to the DFH direction. This correlation was not clear (Figure 10); the HC shows incoherent directions among sites, although within-site clustering is reasonable. This is in sharp contrast with the results of McElhinny & Senanayake (1980), where all the 6 sites revealed well-clustered DFH directions.

Because 4 out of 12 sites are likely to be affected by lightning strikes, the other sites may be contaminated by IRM. Nonetheless, we argue that lightning strikes alone is not adequate to explain the incoherent HC directions. The site GL3-15 revealed apparently antipodal HC directions. This is difficult to be produced by lightning strikes, and more likely to result from prolonged remanence acquisition over polarity reversal(s), supporting the secondary origin of hematite. The site GL3-12 includes three drill cores and a hand sample collected from an area of ∼6 m. All of them shows reasonably coherent MC and HC directions. Thus, the HC as well as the MC direction in GL3-12, which happens to agree with DFH, does not seem to be affected by lightning strikes.

We also point out that the AF demagnetization behavior of HC is different from that of DFH. McElhinny & Senanayake (1980) interpreted the component demagnetized at 40 - 200 mT as DFH carried by hematite. However, our comparison between thermal- and AF demagnetization revealed that the re-

manence of hematite (HC) is hardly demagnetized up to 150 mT (Figure 9). Therefore, we infer that DFH originally defined by McElhinny & Senanayake (1980) includes remanence carried by high coercivity (titano)magnetite.

5.2.2. (titano)magnetite components (MC, LMC, and HMC)

McElhinny & Senanayake (1980) assigned only one component for titanomagnetite except for an unstable overprint in their thermal demagnetization. However, our data as well as those of Herrero-Bervera et al. (2016) revealed that the Duffer Formation dacite contains titanomagnetite and magnetite with Curie temperatures of ∼350 °C and ∼590 °C, respectively, and they record distinct remanence directions. LMC unblocks sharply at ∼350 °C (Figure 8), and we interpret that this component is carried by titanomagnetite. On the other hand, MC and HMC extend up to ∼500 °C and ∼590 °C, respectively, so we interpret that these components are carried by magnetite.

As discussed in the Magnetic mineralogy section, rock magnetic and microscopic data suggest that magnetite has lower coercivity than titanomagnetite on average. This explains the observation that MC is not separated in AF demagnetization and apparently demagnetized below 30 mT (Figure 9). On the other hand, at least one sample (GL3-16) showed HMC in 60 - 150 mT, suggesting that some magnetite is of high coercivity.

It is also interesting to note that the AF demagnetization behavior of GL3-16 is similar to the result presented by McElhinny & Senanayake (1980). They called a component demagnetized in 40 - 200 mT as DFH, which is supposed to be carried by hematite. On the other hand, our data showed that the component demagnetized at 60 - 150 mT was HMC carried by magnetite (Figure 8), so we interpret that HMC is correlatebale to DFH

even though it is carried by magnetite. High among-site dispersion prevent paleomagnetic tests to constrain the age of HMC. Assuming the original inference that DFH is a secondary component (McElhinny & Senanayake, 1980), our interpretation indicates that the columnar dacite contains high coercivity and high unblocking temperature secondary magnetite, which can be formed by alteration of mafic minerals (Figure 8b). This would limit the use of this material in paleointensity studies.

5.2.3. Implications for the 'primary' remanence

The putative primary remanence DFM was reported from both thermal- and AF demagnetization in $250-500\,^{\circ}\mathrm{C}$ and $10-40$ mT range, respectively (McElhinny & Senanayake, 1980). On the basis of unblocking temperature and coercivity, they may be correlated with MC and LMC in our data (Table 2; Figure 8). Although MC and LMC are carried by different minerals of magnetite and titanomagnetite, respectively, both oxide were observed as magmatic crystals (Figure 8). While this does not provide evidence for the age of DFM, it is consistent with the near primary age of the component.

Small number of successful sites and apparently high among-site scatter prevent directional comparison among LMC, MC, and DFM, and suggest the need for caution in interpretation. Nonetheless, if LMC corresponds to DFM, and if they are nearly primary as suggested by McElhinny & Senanayake (1980), clearly the rocks should not have experienced heating above $\sim 350\,^{\circ}\mathrm{C}$ for $\sim$3.47 billion years, and probably they have been kept below $\sim 250\,^{\circ}\mathrm{C}$ to explain the full range of the unblocking temperature. This would open a way to test the age of the remanence through thermochronology. Using Ar ages collected over a $\sim 80 \times 80$ km area southwest from the columnar dacite, Zegers

et al. (1999) showed that some sites have been kept below the Ar closure temperature of hornblende (∼500 °C) for ∼3.45 billion years. On the other hand, many other sites revealed evidence for reheating at ∼2.9 Ga, which was attributed to the post tectonic granite intrusion in the Shaw Complex (Bickle et al., 1989). Lower temperature chronology is not available except for single site within the Corunna Downs Complex which shows reheating above 300 °C at ∼2.9 Ga (Zegers et al., 1999). More thermochronological data from the area close to the columnar dacite can put constraints on the oldest paleomagnetic record.

6. Conclusions

Despite of its massive appearance, the columnar dacite of the Duffer Formation is magnetically heterogeneous. Bulk magnetic susceptibility varies by a factor of ∼50, with low susceptibility sites dominated by hematite and high susceptibility sites dominated by magnetite and titanomagnetite with Curie temperature of ∼350 °C. Under SEM, titanomagnetite with Ti/Fe of ∼0.14 were observed as fine intergrowth with Ti oxide. Magnetite mainly occurs as relatively large discrete grains. Two distinct grain size populations of (titano)magnetite were also indicated in the bimodal coercivity distribution below 100 mT.

Four remanence components were identified in thermal demagnetization: MC that unblocks at $200 - 500$ °C, HC at ∼690 °C, LMC at $200 - 350$ °C, and HMC at $500 - 590$ °C. Rock magnetic data indicate that these components are carried by coarse-grained magnetite, hematite, titanomagnetite, and fine-grained magnetite, respectively. Together with AF demagnetiza-

tion results and rock magnetic data, we proposed more complex remanence carriers than the original study of McElhinny & Senanayake (1980); the secondary component DFH is likely to be carried by fine-grained magnetite as well as hematite, and the putative primary component DFM may be carried by coarse-grained magnetite and titanomagnetite. Microscopic observations showed that coarse-grained magnetite and titanomagnetite are primary crystals, although this does not necessarily indicate they preserve primary remanence. The remanence directions of all components revealed higher scatter than the previous studies, suggesting the need for caution in interpretation. More systematic investigation is needed to identify representative remanence directions. The low unblocking temperature of tittanomagnetite ($200 - 350\,^{\circ}\mathrm{C}$) suggests that if their remanence is primary, the rocks must have kept below $\sim$250 °C for $\sim$3.47 billion years.

Acknowledgement

We are grateful to Atlas Iron for permission to work in the area. We thank two anonymous reviewers for their constructive comments. YU thanks Aguri Irisawa for the assistance in the lab. This research was supported by JSPS KAKENHI Grant Numbers JP26302004, JP15H03740, JP15H03741,JP15H05468, JP17H04855, and JP17H06455.

Data Availability

Data are uploaded in zenodo repository (doi: ———).

References

Arndt, N. T., Nelson, D. R., Compston, W., Trendall, A. F., & Thorne, A. M. (1991). The age of the Fortescue Group, Hamersley Basin, Western Australia, from ion microprobe zircon UPb results. *Australian Journal of Earth Sciences*, *38*, 261–281. doi:10.1080/08120099108727971.

Bickle, M. J., Bettenay, L. F., Chapman, H. J., Groves, D. I., McNaughton, N. J., Campbell, I. H., & de Laeter, J. R. (1989). The age and origin of younger granitic plutons of the Shaw Batholith in the Archaean Pilbara Block, Western Australia. *Contributions to Mineralogy and Petrology*, *101*, 361–376. doi:10.1007/BF00375320.

Biggin, A. J., de Wit, M. J., Langereis, C. G., Zegers, T. E., Voûte, S., Dekkers, M. J., & Drost, K. (2011). Palaeomagnetism of Archaean rocks of the Onverwacht Group, Barberton Greenstone Belt (southern Africa): Evidence for a stable and potentially reversing geomagnetic field at ca. 3.5 Ga. *Earth and Planetary Science Letters*, *302*, 314–328. doi:10.1016/J.EPSL.2010.12.024.

Bleil, U., & Petersen, N. (1982). Magnetic properties of natural minerals. In G. Angenheister (Ed.), *Numerical Data and Functional Relationships in Science and Technology* (pp. 308–365). New York: Springer.

Bradley, K., Weiss, B. P., & Buick, R. (2015). Records of geomagnetism, climate, and tectonics across a Paleoarchean erosion surface. *Earth and Planetary Science Letters*, *419*, 1–13. doi:10.1016/J.EPSL.2015.03.008.

Davies, C., Pozzo, M., Gubbins, D., & Alfè, D. (2015). Constraints from material properties on the dynamics and evolution of Earth's core. *Nature Geoscience*, *8*, 678–685. doi:10.1038/ngeo2492.

Egli, R. (2013). VARIFORC: An optimized protocol for calculating non-regular first-order reversal curve (FORC) diagrams. *Global and Planetary Change*, *110*, 302–320. doi:10.1016/j.gloplacha.2013.08.003.

Egli, R., Chen, A. P., Winklhofer, M., Kodama, K. P., & Horng, C.-S. (2010). Detection of noninteracting single domain particles using first-order reversal curve diagrams. *Geochemistry, Geophysics, Geosystems*, *11*. doi:10.1029/2009GC002916.

Hale, C., & Dunlop, D. (1984). Evidence for an Early Archean Geomagnetic Field: A paleomagnetic study of the Komati Formation, Barberton Greenstone Belt, South Africa. *Geophysical Research Letters*, *11*, 97–100. doi:10.1029/GL011i002p00097.

Herrero-Bervera, E., Krasa, D., & Van Kranendonk, M. J. (2016). A whole rock absolute paleointensity determination of dacites from the Duffer Formation (ca. 3.467 Ga) of the Pilbara Craton, Australia: An impossible task? *Physics of the Earth and Planetary Interiors*, *258*, 51–62. doi:10.1016/J.PEPI.2016.07.001.

Hickman, A., & Van Kranendonk, M. (2008). Marble Bar, WA Sheet 2855: Geological Survey of Western Australia, 1:100,000 Geological Series. The Geological Survey of Western Australia, East Perth, WA.

Kirschvink, J. (1980). The least-squares line and plane and the analysis of palaeomagnetic data. *Geophysical Journal International*, *62*, 699–718. doi:10.1111/j.1365-246X.1980.tb02601.x.

Layer, P. W., Kröner, A., & McWilliams, M. (1996). An archean geomagnetic reversal in the Kaap Valley pluton, South Africa. *Science*, *273*, 943–946. doi:10.1126/science.273.5277.943.

Lowrie, W. (1990). Identification of ferromagnetic minerals in a rock by coercivity and unblocking temperature properties. *Geophysical Research Letters*, *17*, 159–162. doi:10.1029/GL017I002P00159.

Lurcock, P. C., & Wilson, G. S. (2012). Puffinplot: A versatile, user-friendly program for paleomagnetic analysis. *Geochemistry, Geophysics, Geosystems*, *13*. doi:10.1029/2012GC004098.

McElhinny, M. W., & Senanayake, W. E. (1980). Paleomagnetic evidence for the existence of the geomagnetic field 3.5 Ga ago. *Journal of Geophysical Research: Solid Earth*, *85*, 3523–3528. doi:10.1029/JB085iB07p03523.

Nelson, D. (2001). *Compilation of geochronology data, 2001*. The Geological Survey of Western Australia.

Pidgeon, R. (1978). 3450-m.y.-old volcanics in the Archaean layered greenstone succession of the Pilbara Block, Western Australia. *Earth and Planetary Science Letters*, *37*, 421–428. doi:10.1016/0012-821X(78)90057-2.

Schmidt, P. W. (2014). A review of Precambrian palaeomagnetism of Australia: Palaeogeography, supercontinents, glaciations and true polar wan-

der. *Gondwana Research*, *25*, 1164–1185. doi:10.1016/J.GR.2013.12.007.

Suganuma, Y., Hamano, Y., Niitsuma, S., Hoashi, M., Hisamitsu, T., Niitsuma, N., Kodama, K., & Nedachi, M. (2006). Paleomagnetism of the Marble Bar Chert Member, Western Australia: Implications for apparent polar wander path for Pilbara craton during Archean time. *Earth and Planetary Science Letters*, *252*, 360–371. doi:10.1016/J.EPSL.2006.10.003.

Tarduno, J. A., Cottrell, R. D., Watkeys, M. K., & Bauch, D. (2007). Geomagnetic field strength 3.2 billion years ago recorded by single silicate crystals. *Nature*, *446*, 657–660. doi:10.1038/nature05667.

Usui, Y., Tarduno, J. A., Watkeys, M., Hofmann, A., & Cottrell, R. D. (2009). Evidence for a 3.45-billion-year-old magnetic remanence: Hints of an ancient geodynamo from conglomerates of South Africa. *Geochemistry, Geophysics, Geosystems*, *10*. doi:10.1029/2009GC002496.

Yoshihara, A., & Hamano, Y. (2004). Paleomagnetic constraints on the Archean geomagnetic field intensity obtained from komatiites of the Barberton and Belingwe greenstone belts, South Africa and Zimbabwe. *Precambrian Research*, *131*, 111–142. doi:10.1016/J.PRECAMRES.2004.01.003.

Zegers, T., Wijbrans, J., & White, S. (1999). $^{40}Ar/^{39}Ar$ age constraints on tectonothermal events in the Shaw area of the eastern Pilbara granite-greenstone terrain (W Australia): 700 Ma of Archean tectonic evolution. *Tectonophysics*, *311*, 45–81. doi:10.1016/S0040-1951(99)00157-2.